Angewandte Chemie International Edition

Angewandte International Edition Chemie

How to cite: *Angew. Chem. Int. Ed.* **2026**, e26012
doi.org/10.1002/anie.202526012

RESEARCH ARTICLE OPEN ACCESS

Delayed Halide-Rich Molecular Passivation of $CsPbCl_3$ Perovskite Nanocrystals Enables Bright Violet Light-Emitting Diodes

Nadesh Fiuza-Maneiro[1] | Junzhi Ye[2,3] | Woo Hyeon Jeong[3,4] | Rui Xu[5] | Qingyu Wang[6] | Dong Yoon Chung[3] | Robert A. Taylor[6] | Iago López-Fernández[1] | Bofeng Xue[7] | Akshay Rao[7] | Bo Ram Lee[4] | Yunwei Zhang[5] | Robert L. Z. Hoye[3] | Sergio Gómez-Graña[1] | Lakshminarayana Polavarapu[1]

[1]CINBIO, Universidade de Vigo, Department of Physical Chemistry, Campus Universitario As Lagoas-Marcosende, Universidade Devigo, Vigo, Spain | [2]Institute of Polymer Optoelectronic Materials and Devices, Guangdong Basic Research Center of Excellence for Energy & Information Polymer Materials, State Key Laboratory of Luminescent Materials and Devices, School of Materials Science and Engineering, South China University of Technology, Guangzhou, China | [3]Inorganic Chemistry Laboratory, University of Oxford, Oxford, UK | [4]School of Advanced Materials Science and Engineering, Sungkyunkwan University, Suwon, Republic of Korea | [5]School of Physics, Sun Yat-sen University, Guangzhou, China | [6]Clarendon Laboratory, Department of Physics, University of Oxford, Oxford, UK | [7]Cavendish Laboratory, University of Cambridge, Cambridge, United Kingdom

Correspondence: Junzhi Ye (junzhiye1994@scut.edu.cn) | Sergio Gómez-Graña (segomez@uvigo.gal) | Lakshminarayana Polavarapu (lakshmi@uvigo.gal)

Received: 24 November 2025 | **Revised:** 5 April 2026 | **Accepted:** 7 April 2026

Keywords: $CsPbCl_3$ NCs | LEDs | passivation | transient-absorption | violet-blue emission

ABSTRACT

$CsPbCl_3$ perovskite nanocrystals (NCs) are promising violet emitters owing to their narrow emission and high color purity, but their low defect tolerance demands careful passivation to achieve high photoluminescence quantum yield (PLQY), and typically only for fresh $CsPbCl_3$ NCs. Here, we report a delayed dual-passivation pathway in $CsPbCl_3$ NCs induced by the halide-rich molecular reagent phosphorus oxychloride ($POCl_3$), which unexpectedly yields a strong time-dependent PLQY enhancement instead of the rapid degradation usually observed. $POCl_3$ gradually decomposes into P- and Cl-containing species, enabling a controlled release of excess halides that autonomously passivates halide vacancies in a self-regulated manner. This dynamic self-healing process boosts the PLQY of colloidal $CsPbCl_3$ NCs by over 40-fold relative to pristine samples and sustains high violet emission efficiencies for more than 2 months of storage under ambient conditions. Spectroscopic measurements and calculations indicate that both liberated Cl^- and in situ—formed phosphonic species passivate halide vacancies and Pb^{2+} dangling bonds, suppressing mid-gap defect states. The resulting self-passivated NCs deliver a luminance of 409 cd m^{-2}, the highest reported for $CsPbCl_3$-based violet emitters. These results establish halide-rich dual passivators such as $POCl_3$ as powerful tools for long-term defect control in chloride perovskite NCs and for robust, bright violet-LEDs.

1 | Introduction

Over the past decade, lead halide perovskite (LHP) nanocrystals (NCs) have gained considerable attention due to their highly advantageous and versatile optoelectronic properties, including high quantum yields, sharp light emission, and widely-tunable emission across the violet, visible, and near-infrared wavelength range [1]. One of the advantages over conventional semicon-

Nadesh Fiuza-Maneiro and Junzhi Ye contributed equally to this work.

ductors is that they are defect-tolerant and can maintain their remarkable optoelectronic properties, even with high defect density. Consequently, LHPs have gained popularity and are emerging in numerous applications such as light-emitting diodes (LEDs), solar cells, lasers and others [1–6].

The defect tolerance of perovskites is largely attributed to the predominance of shallow traps with low capture cross-sections [7]. Consequently, trap-assisted recombination is substantially suppressed, even under conditions of high defect density. The type of halide and the lattice characteristics influence defect behavior as well. As the halide size decreases from iodine to chlorine, the lattice parameter reduces, leading to shorter lead–halide bonds. The increased ionicity of these bonds further results in a wider bandgap and lower electron affinity, which makes the formation of deep traps more likely in $CsPbCl_3$ than in iodide-based counterparts [8–10]. As a result, oleylammonium (OAm)-capped $CsPbCl_3$ NCs typically exhibit PLQYs around 1%–3%, whereas $CsPbBr_3$ and $CsPbI_3$ NCs can reach nearly 100% [11–14]. For this reason, most studies involve mixed Br/Cl NCs or blue emissive $CsPbBr_3$ nanoplatelets (NPls) rather than chloride-based NCs [15–19]. However, this alternative remains a non-viable option due to the halide segregation in case of mixed halide composition [20] or its high defect density in the case of NPls, resulting from its high surface-to-volume ratio. This defect density not only impairs its quantum yields but also leads to poor colloidal stability, which is further compromised in the solid state [6, 7]. In addition, the use of NPls has limitations when it comes to archiving emissions in the violet range (400–420 nm) [21]. Nevertheless, over time, due to their ionic nature, the ligands can detach, either as a result of intrinsic structural factors or external conditions such as aging, washing, or dilution. This can lead to adverse effects on both the luminescence efficiency of the NCs and their overall stability, a typical behavior seen in LHP NCs [22, 23].

Therefore, achieving high-quality NCs with high PLQY and long-term stability, especially for $CsPbCl_3$ NCs, is a grand challenge for the development of violet and blue LEDs [24]. Numerous studies have demonstrated that, in the pursuit of enhanced stability and luminescence, the application of ligands or reagents with high surface energy affinity can effectively passivate defects in NCs [25–36]. Despite extensive research on bromide and iodide NCs, as well as NPls [15], the detailed investigation of $CsPbCl_3$ NCs remains limited. Several recent studies have reported notable improvements in PLQY upon the addition of divalent metal halides [26, 37] and dopants such as $CdCl_2$ [38, 39] or YCl_3 [31]. However, PLQY values are typically measured only in freshly prepared samples, without any evaluation of their long-term stability. In previous studies conducted within our group [40], we explored passivation strategies using various ligands and metal halides. These efforts allowed us to identify halide vacancies as the primary defects that most significantly degrade the optoelectronic properties of chloride-based NCs. Based on our previous findings, where phosphorus-based compounds and chloride sources were shown to most effectively enhance the photoluminescence of $CsPbCl_3$ NCs synthesized by a typical hot injection synthesis [21], we introduced a single passivator containing both elements (phosphorus and chloride) to achieve synergistic performance enhancement. Therefore, we selected phosphorus oxychloride, $POCl_3$, a highly reactive compound with high Lewis acidity. To evaluate its effectiveness, we carried out two types of passivation: one in situ, by incorporating the reagent directly into the colloidal sample during synthesis, and another through a post-synthetic treatment. Through these approaches, we achieved a remarkable 55-fold enhancement in the PL of $CsPbCl_3$ NCs from 0.91 ± 0.1% PLQY for pristine to 40.9 ± 2.4% PLQY for $POCl_3$-treated, remarkably maintaining high PLQY for over 2 months under ambient conditions. This advancement surpasses previously-reported stabilities with alternative strategies [29, 40].

2 | Results and Discussion

The synthetic strategy we used here for $CsPbCl_3$ NCs was inspired by a typical hot injection synthesis following the standard procedure [21], with the additional incorporation of $POCl_3$ into the reaction mixture prior to the injection of Cs-oleate (Figure 1a and see experimental section in Supporting Information for more details). The idea behind the use of this halide-rich molecule is to investigate whether it promotes the passivation of deep traps through passivation of halide vacancies (see Figure S1 for details on the PLQY measurement protocol). The $POCl_3$-treated NCs have a photoluminescence (PL) peak at ~401 nm wavelength, comparable to the reported pristine $CsPbCl_3$ NCs [40], but with a reduced full-width half maximum (FWHM) of 13.6 nm, indicating high size monodispersity and low surface disorder [41, 42], typically observed in trap-free NCs (see Figure S2 for more STEM images). The average particle size was measured as 6.19 ± 0.07 nm, showing a smaller size distribution than the typical $CsPbCl_3$ pristine NCs (Figures 1b and S3). Comparison of PL intensities revealed that the $POCl_3$-treated NCs displayed a 40-fold increase in PLQY relative to the pristine sample (Figure 1c). The enhanced luminescence reflected in a significant increase in lifetime was observed, rising from 2.27 to 14.28 ns at 41.88 $\mu J/cm^2$ fluence (Figure 1d), which is typically due to reduced nonradiative decay. XRD analysis indicated that the cubic-phase structure was preserved in the $POCl_3$-treated sample, while EDX studies confirmed the presence of phosphorous atoms (P) in the NCs (Figure S4a,c). Furthermore, we investigated whether the incorporation of $POCl_3$ enhanced colloidal stability against purification using ethyl acetate (EtOAc) antisolvent, a key requirement for LED device fabrication. By comparing pristine NCs with those treated with $POCl_3$, we observed higher luminescence in the treated samples after three washes, suggesting that the passivating agent helps improve the stability by filling traps that could otherwise lead to non-radiative recombination (Figure S4b).

To substantiate the role played by the reagent, we also compared different passivation methods, including post-synthetic passivation, which required the prior preparation of $CsPbCl_3$ NCs. The pristine NCs were synthesized via a conventional hot-injection method at 180°C, yielding particles with an average size of 6.24 ± 0.23 nm. Their PL spectrum displays a peak at 401 nm with a photoluminescence quantum yield (PLQY) of approximately 1% and a full width at half maximum (FWHM) of 15.7 nm (Figures S5 and S6). Subsequently, post-synthetic passivation was carried out by adding 2 mM solutions of POX_3 (X = Cl, Br) in toluene to the pristine NC solution at a 1.66:1 volume ratio, followed by a minute of sonication. EtOAc was then added as an antisolvent to precipitate the NCs, which were centrifuged at 6 000 rpm for 10 min to remove excess ligands. The resulting precipitate

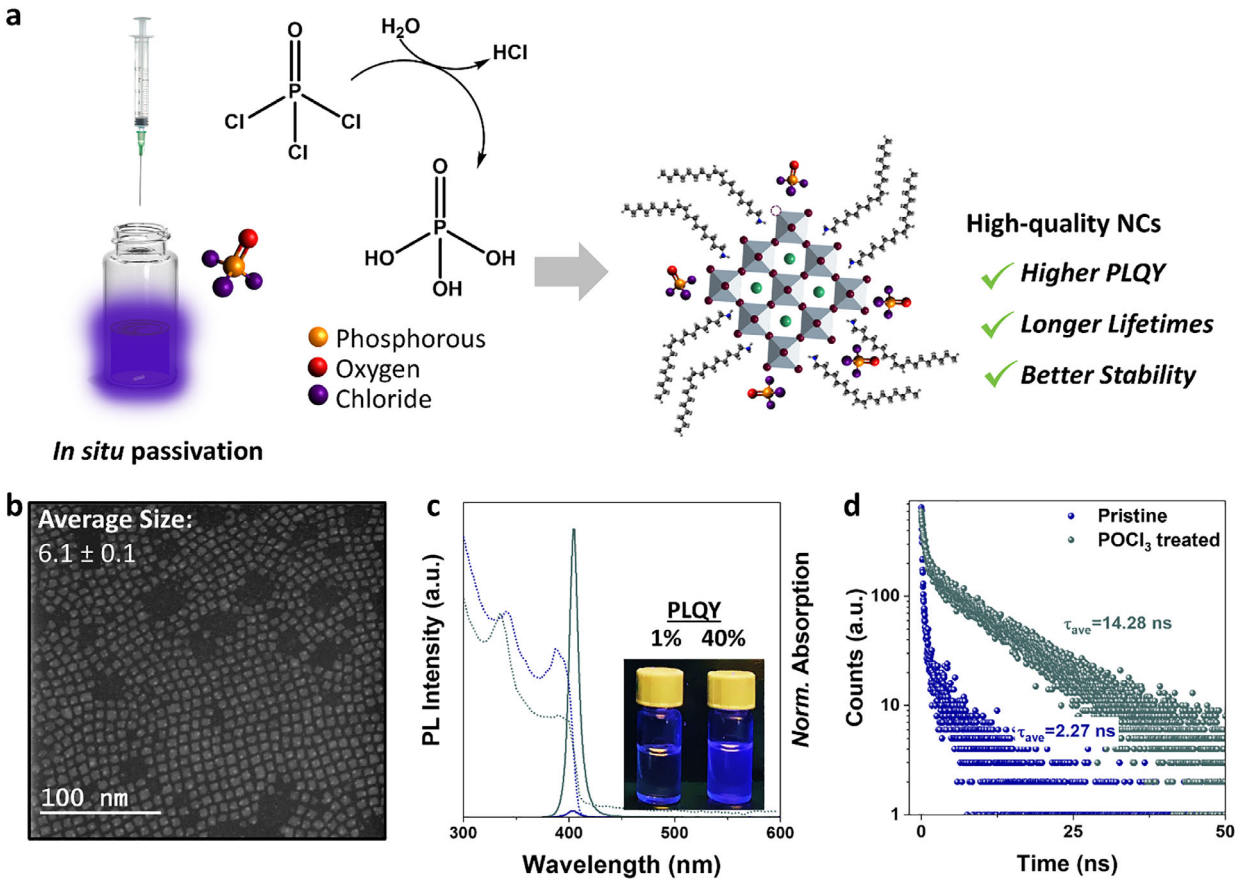

FIGURE 1 | (a) Scheme of in situ passivation mechanism with $POCl_3$ on $CsPbCl_3$ NCs, where we introduce the $POCl_3$ passivator directly in the precursor solution. The $POCl_3$ molecules added during the synthesis will gradually release Cl^- ions and form phosphate and phosphoric acid to repair the Cl vacancies leading to surface passivated crystals; accordingly, the data presented in the following graphs correspond to samples aged 15 days. (b) STEM image of $CsPbCl_3$ NCs treated with $POCl_3$. (c) Normalized PL Intensity to the absorption at excitation wavelength and absorption normalized to the maximum of pristine $CsPbCl_3$ and $POCl_3$ treated NCs. (d) Time-resolved photoluminescence decay of pristine and $POCl_3$ treated NC drop-cast films. The excitation source is a nanosecond pulsed laser with a 350 nm wavelength (41.88 μJ/cm^2 fluence).

was redispersed in toluene for further characterization. After treating the pristine NCs with $POCl_3$, we observed a significant increase in the PLQY by approximately 25-fold (PLQY for $POCl_3$ passivated sample is 22.9 ± 3.6), accompanied by a substantial increase of the lifetime by 3-fold, reaching 6.56 ns (Figure S6). However, despite this notable improvement, the results did not reach the enhancement level obtained for the in situ passivation colloidal synthesis. Nevertheless, post-synthetic passivation can still be considered an effective strategy for repairing damaged NCs. We considered passivating $CsPbBr_3$ NCs using the bromide analogue, $POBr_3$. This treatment proved to be effective as a passivating agent, although to a lesser extent than in the case of chloride-based perovskites (Figure S7a). This observation is consistent with the fact that $CsPbCl_3$ NCs possess a higher density of deep traps [7–10, 43]. Upon performing passivation on NCs of the different halide composition, namely, using $POBr_3$ on $CsPbCl_3$ NCs and $POCl_3$ on $CsPbBr_3$ NCs, we observed that these passivating agents were not only effective in inducing partial anion exchange, but also led to an enhancement of the PL, attributable to the simultaneous passivation of trap states (Figure S7b,c). These results suggest that the POX_3 molecule easily releases halide ions when they are in contact with perovskite NCs. Nevertheless, their efficiency as anion-exchange agents is lower compared to other commonly employed strategies.

After determining that in situ passivation is significantly more effective than post-synthetic passivation, we conducted a more detailed investigation of this process to understand the origin of the dramatic enhancement of the PLQY. As an initial step, we evaluated its effectiveness as a passivating agent over time upon ambient storage (16°C–20°C, 45%–60% relative humidity) of the purified NCs. The results revealed a remarkable finding: a progressive increase in quantum yield was observed as time elapsed shown in Figures 2a and S8 despite washing conditions, a novel behavior that, to the best of our knowledge, has not been previously reported for $CsPbCl_3$ NCs. Initially, this increase occurs progressively, reaching a maximum approximately 15 days after synthesis, which suggests a gradual passivation of chloride traps. To gain deeper insight into the possible underlying mechanism, we performed phosphorus ^{31}P NMR spectroscopy measurements shown in Figure 2b, comparing pure phosphorus oxychloride with a perovskite sample treated with it, both immediately after treatment and after 7 days. When comparing the signals of $POCl_3$ with those of the treated NC sample, we observe the appearance of several new resonances in the fresh sample at lower chemical shift values (upfield), around −11.2 and −24.7 ppm. These features suggest the presence of condensed phosphates such as pyro- and polyphosphates ($[PO_4]^{3-}$), arising from the decomposition products of $POCl_3$ (Table S1). Additionally, a shift of the $POCl_3$

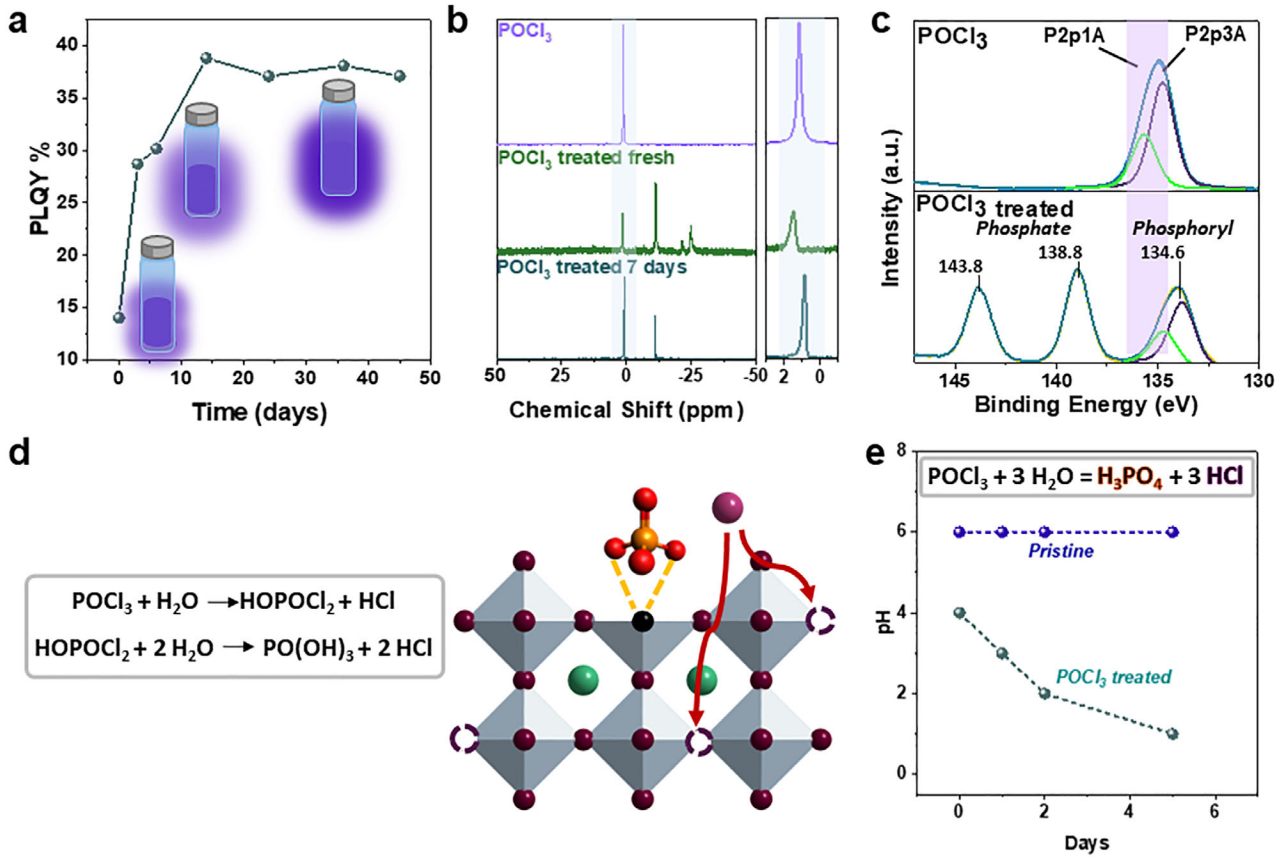

FIGURE 2 | (a) PLQY over aging time for colloidal $CsPbCl_3$ NC solutions prepared by in situ passivation with $POCl_3$. (b) ^{31}P NMR spectra for the pure $POCl_3$, and $POCl_3$ treated sample, fresh and after 7 days. (c) XPS spectra of phosphorous core levels for $POCl_3$ and the treated NCs. (d) Scheme of dual passivation mechanism of $CsPbCl_3$ NCs where chloride is labeled in purple and the group POOH in red and orange. The $POCl_3$ gradually decomposes into phosphoryl group (—P (═O)(—O^-)$_2$) and phosphoric acid (H_3PO_4) (e) pH over time of pristine and $POCl_3$ treated sample with a noticeable increase in acidity overtime due to the formation of phosphoric acid.

signal to 1.56 ppm is observed, consistent with its hydrolysis to phosphate ($[PO_4]^{3-}$). In contrast, in the one-week-old sample, some of the high-field signals have disappeared, leaving only the resonance at −11.08 ppm, along with a low-field signal around 0.85 ppm, which indicates the presence of phosphate and a phosphoryl group (—P (═O)(—O^-)$_2$), both attributable to decomposition products from the hydrolysis of $POCl_3$. However, determining the origin of these signals is challenging due to the high versatility of phosphorus chemistry, which can lead to the formation of numerous species and corresponding resonances. We then examined x-ray photoelectron spectroscopy (XPS) of these samples, focusing on the behavior of phosphorus in $POCl_3$ in the treated sample. A noticeable shift in binding energies was observed, with a new feature appearing at lower binding energy around 134.6 eV, typically attributed to the phosphoryl group. In addition, a signal at approximately 138.8 eV can be assigned to the phosphate group (Figure 2c). Interestingly, an additional peak emerges at 143.8 eV, which may be associated with the coordination of one of these phosphorus-containing groups to the lead atom, where we expect a shift to high binding energies due to the withdrawal of the electron density from phosphorus, which makes the P slightly more electron-deficient. In addition, the O 1s XPS data reveal clear evidence for the early stages of $POCl_3$ hydrolysis. In the O 1s region, two contributions are observed: a peak at 531.33 eV, assigned to P═O phosphoryl groups, and a second component at 532.80 eV, indicative of the initial formation of P—OH species (Figure S9) [44]. These observations provide insight into the possible hydrolysis of $POCl_3$: [45–47] being a highly unstable reagent, it can decompose in the presence of trace amounts of water, forming phosphoric acid and hydrochloric acid via a phosphoryl intermediate (Figure 2d). To verify whether a mildly acidic environment was forming in the sample, we conducted a time-resolved pH analysis. Compared to the pristine sample, the treated solution was significantly more acidic from the outset, and its acidity continued to increase over the following weeks (Figures 2e and S10). We also investigated whether the gradual filling of traps was driven solely by chlorine generated during the decomposition of $POCl_3$, or if incorporation of phosphorus into the structure was also occurring. The sample composition was analyzed via inductively coupled plasma mass spectrometry (ICP). A fresh $CsPbCl_3$ sample treated with $POCl_3$ was washed to remove any excess phosphorus from the medium, ensuring that only phosphorus incorporated into the lattice was measured. This was compared with a sample aged for 2 weeks, revealing a slight increase in the phosphorus content (Table S2). These results suggest that delayed passivation also occurs through the incorporation of phosphorus atoms.

To understand the effect of passivation on the optoelectronic properties of $CsPbCl_3$ NCs, we calculated the projected density

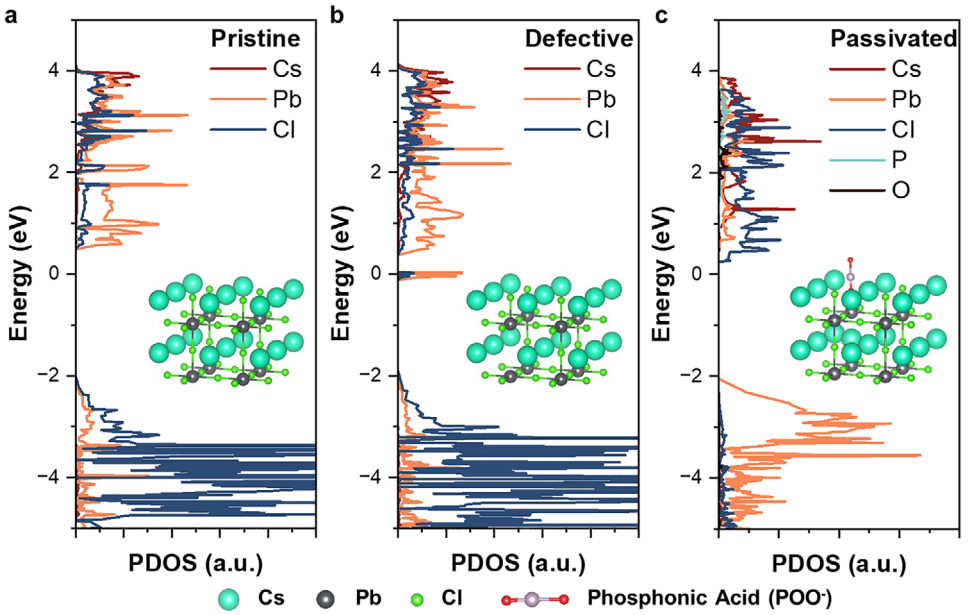

FIGURE 3 | Calculated density of states for pristine $CsPbCl_3$ NCs, defective $CsPbCl_3$ NCs and passivated $CsPbCl_3$ NCs with a phosphonic acid functional group. The insets show the structure of the unit cells. The supercell used is 2 × 2 × 1. There is clear mid gap defect states for the defective supercell with Cl missing. The release of Cl ions and phosphoric acid group from $POCl_3$ successfully remove the mid-gap states after recompensating the Cl vacancies and coordinating the unbound Pb^{2+} states.

of states (PDOS) of the pristine (no defects), defective (with Cl vacancies) and passivated (phosphonic acid) cells shown in Figure 3a–c. When there is no defect present, there is no additional density of states between the conduction band minimum and valence band maximum as shown in Figure 3a. When the Cl-vacancies were introduced during the NC purification process for device fabrication, it led to the formation of deep trap states (approximately 0.4 eV below CBM) in the middle of the bandgap, as shown in Figure 3b. These additional trap states can be mediated when the oxygen (O) atom from the phosphonic acid group re-coordinates with the Pb at where the Cl is removed, as shown in Figure 3c. To further test our hypothesis regarding the passivation species, the total density of states for different passivators such as $POCl_3$, POOH, and POCl are calculated and shown in Figure S11. In these cases, the mid-gap defects cannot be fully passivated. This aligns with our ^{31}P NMR analysis, which suggests that the formation of deprotonated phosphonic acid would be the final passivator that mediates the deep traps and leads to the increase in PLQY over time. Notably, the $POCl_3$ treatment does not induce a significant shift in the steady-state absorption or emission spectra, indicating that the bandgap and band-edge energy levels of the nanocrystals remain largely unchanged. Instead, the dominant effect is the passivation of surface defect states, which reduces mid-gap trap densities. This is expected to alleviate Fermi-level pinning and improve charge-carrier extraction in device architectures, without significantly altering the intrinsic band alignment. Therefore, the enhanced optoelectronic performance arises primarily from suppressed nonradiative recombination rather than changes in the band structure based on our optical measurements and DFT calculations.

Furthermore, transient absorption (TA) spectroscopy is used to understand the effect of passivation on charge-carrier kinetics. The 2D heat maps of the pristine and passivated solution samples are shown in Figure 4a,d. It clearly shows that the width of the ground state bleach (GSB) signal around 390–405 nm is narrower when treated with $POCl_3$. This would be due to improved size distribution of the NCs, reducing surface disorder and removing shallow traps [41, 42]. This can also be seen in Figure 4b,e, where the FWHM of the GSB peaks becomes much narrower when treated with $POCl_3$. At higher pump fluence, a weak splitting of the bleach feature is observed in the 405–420 nm range for both pristine and treated samples, likely due to signals from NCs with different sizes. Since the emission is governed by the exciton recombination (Figure S12), we fit the exciton recombination rate equation (Equations 1 and 2) to the fluence dependent decay curve probed at GSB peaks between 395 and 400 nm shown in Figure 4c,f, where n_{ex} is the density of photo-generated excitons, k_{PL} is the total monomolecular recombination rate ($k_{PL} = \frac{1}{\tau} = k_{rad} + k_{trap}$, where τ is the exciton lifetime at low fluence where exciton–exciton annihilation is negligible), and $n_{ex}(0)$ is the initial exciton density immediately after photo-excitation. Equation 2 is used for fitting the very early decay curve (~100 ps) when there is minimum radiative recombination and the decay is dominated by the exciton–exciton annihilation (k_{Ann}).

$$\frac{dn_{\mathrm{ex}}}{dt} = -k_{\mathrm{PL}} n_{\mathrm{ex}}(t) - \frac{1}{2} k_{\mathrm{Ann}} n_{\mathrm{ex}}(t)^2 \tag{1}$$

$$n_{ex}(t) = \frac{n_{ex}(0)}{1 + \frac{1}{2} k_{ann}.n_{ex}(0).t} \tag{2}$$

The fitted result shows that the passivated samples have a smaller annihilation rate ($2.09 \pm 0.06\ \mathrm{cm^2\ s^{-1}}$) compared to the pristine sample ($3.54 \pm 0.13\ \mathrm{cm^2\ s^{-1}}$) (Table 1). The smaller k_{Ann} obtained after $POCl_3$ treatment indicates suppressed exciton–exciton interactions. Physically, this can be understood as a consequence of

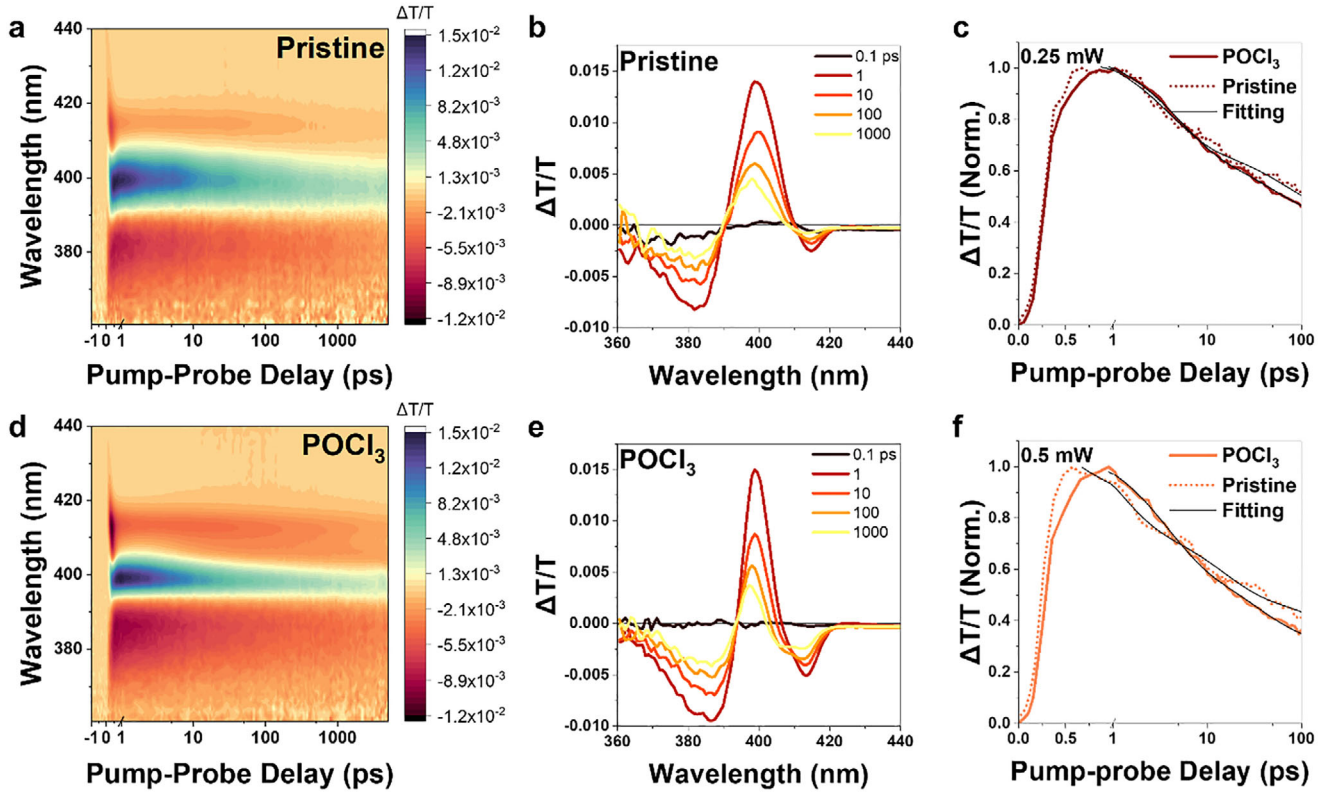

FIGURE 4 | Transient absorption spectroscopy for pristine and passivated $CsPbCl_3$ NCs. (a) TA map of pristine sample at 0.5 mW. (b) TA spectra of the pristine sample at 0.5 mW. (c) Experimental and fitted TA decay curve of pristine and passivated samples probed at 395–405 nm at 0.25 mW. (d) TA map of $POCl_3$-treated sample at 0.5 mW. (e) TA spectra of the passivated sample at 0.5 mW. (f) Experimental and fitted TA decay curve of pristine and passivated samples probed at 395–405 nm at 0.5 mW. The samples are pumped by a 355 nm laser.

TABLE 1 | TA decay fitting for exciton–exciton annihilation kinetics for pristine and passivated samples.

Sample (solution)	k_{Ann} cm^2 s^{-1}
Pristine	3.54 ± 0.13
Passivated	2.09 ± 0.06

surface trap passivation, which reduces the density of defect-mediated interaction sites. As a result, excitons become more uniformly distributed and less likely to undergo diffusion-assisted encounters that lead to annihilation. In addition, improved surface passivation can decrease exciton localization at defective surface regions, thereby lowering the local exciton density and reducing the probability of exciton–exciton annihilation. This matches the observations in other strongly-confined systems, such as nanoplatelets and 2D materials, where exciton populations govern the recombination kinetics [48–50]. In contrast, the higher k_{Ann} is due to higher defect densities of pristine samples, despite the overall lifetime being longer. The high defect densities would trap more excitons at early times (< 10 ps), which increases the probability for two excitons to annihilate. This explains the faster decay for the pristine samples before 10 ps, and this phenomenon is more obvious at higher fluence (0.5 mW), as there are more excitons generated at higher excitation density, it is more likely for the trapped excitons to annihilate, as shown in Figure 4f (for more information, see Figures S13). These early-time TA decay measurements demonstrate clearly that the $POCl_3$ treatment can significantly lower the trap density, aligning well with our observations of the increase in PLQY.

Lastly, we fabricate the $CsPbCl_3$ NC LED devices, addressing an area in which development remains notably underexplored. It is worth noting that the pristine NC samples do not form high-quality films with low current density (shown in Figure S14a) likely due to the presence of more long insulating ligands, and there is no luminance for the pristine NC devices. The device structure is shown in Figure 5a, where PEDOT:PSS and PVK (Poly(9-vinylcarbazole)) serve as the hole injection layer and TPBi serves as the electron injection layer. The current density–voltage curve and luminance are shown in Figure 5b. The turn-on voltage is 3.9 V with a maximum luminance of 409 cd m^{-2}. The maximum external quantum efficiency is 0.11%, as shown in Figure 5c. By introducing $POCl_3$ treatment during NC synthesis, this work achieves the highest luminance reported for $CsPbCl_3$ LEDs compared to previous reports, as evidenced in Figure 5d and Table S3 (EL spectra shown in Figure S14b with EL peak centered at 412 nm). The operational stability of the devices was further evaluated, yielding a T_{50} lifetime of ~40 s at an initial luminance of 100 cd m^{-2} under 5.7 V (Figure S14c), which is close to other strongly confined excitonic emission systems reported, such as perovskite nanoplatelets (T_{50} of 120s) [48]. While these results demonstrate improved material quality and device performance, the limited operational lifetime highlights that stability under electrical bias remains a key challenge for

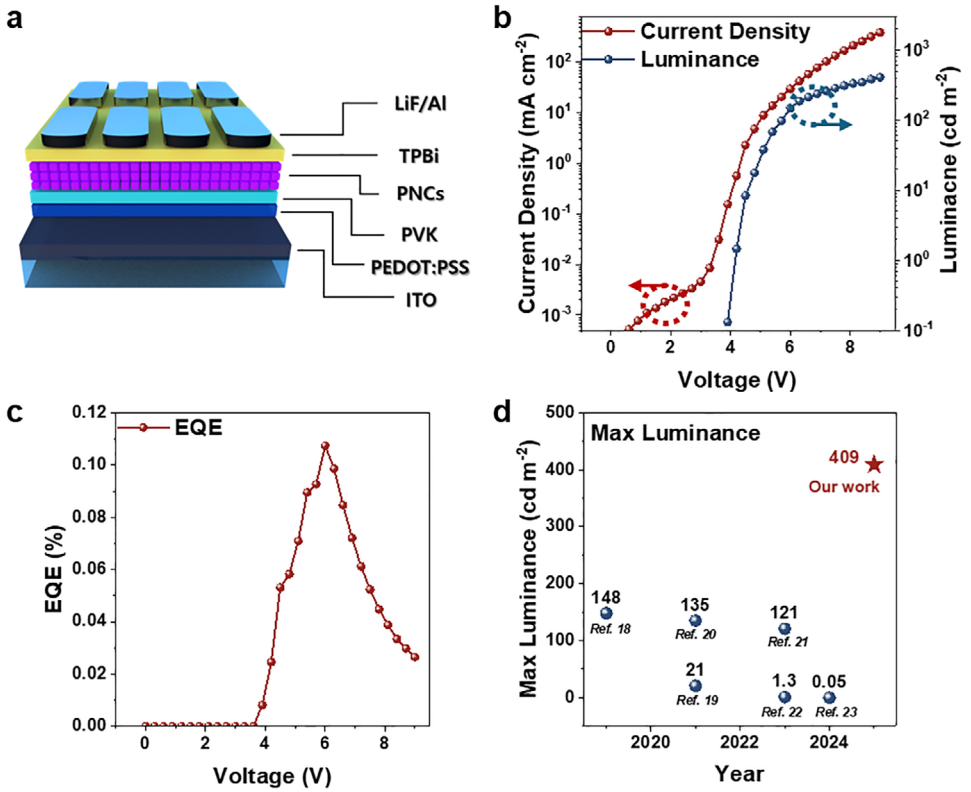

FIGURE 5 | Passivated $CsPbCl_3$ nanocrystal LEDs. (a) LED device structure. (b) Current density/Luminance and voltage curve. (c) Device EQE and voltage curve (d) Maximum luminance of perovskite violet-LEDs of this work and reported values in literature (148) Ref [51], (21) Ref [52],(135) Ref [53], (121) Ref, [54] (1.3) Ref [55] and (0.05) Ref [56].

Cl-based nanocrystal LEDs. These results are encouraging and provide a solid foundation for ongoing efforts around the globe to further develop high-performance violet-blue LEDs.

3 | Conclusion

We demonstrate that $POCl_3$ functions as a halide-rich, self-decomposing passivator that triggers a delayed, sustained defect-healing process in $CsPbCl_3$ nanocrystals. Controlled $POCl_3$ hydrolysis continuously supplies Cl^- while generating phosphonic-acid (P–OH) species that strongly bind under-coordinated Pb^{2+} sites. Time-resolved ^{31}P NMR and pH measurements confirm stepwise hydrolysis and incorporation of P-containing fragments, consistent with a self-regulated, time-dependent passivation mechanism. DFT calculations identify deprotonated phosphonic acids as the most effective surface ligands, eliminating mid-gap trap states by re-coordinating Pb^{2+} dangling bonds. Transient absorption and TRPL kinetics reveal substantially reduced trap densities, in line with the observed ~40-fold increase in PLQY, narrower emission, and high violet emission stability for over 2 months under ambient conditions. At the device level, these self-passivated NCs enable violet LEDs with a record luminance of 409 cd m^{-2}, the highest reported for bright $CsPbCl_3$ emitters. More broadly, these results establish a general design principle for wide-bandgap perovskites: halide-rich, dual-function molecular passivators that gradually release anions while forming robust surface bonds can compensate halide loss, suppress defects, and sustain long-term photostability, offering a practical route to bright, durable, and scalable violet optoelectronics.

Acknowledgements

This work has received funding from the Spanish Agencia Estatal de Investigación (AEI/MCIN) through grants: L.P. acknowledges support from the Spanish Ministerio de Ciencia e Innovación through Ramón y Cajal grant (Grant Number. RYC2018-026103-I), EIC PATHFINDER CHALLEGNES project 101162112 (RADIANT) and a grant from Xunta de Galicia/ERDF (Grant Number. ED431f2021/05). S.G.-G. and L.P. acknowledge the support from MICIU/AEI/10.13039/501100011033 and ERDF/EU (grant nos. PID2023-147567NB-I00, TED2021-131628A-I00 and CNS2022-135531). B.X. thanks the Cambridge Trust, the China Scholarship Council and the Winton Programme for the Physics of Sustainability for funding. W.H.J. acknowledge the support from the National Research Foundation of Korea (NRF) grant funded by the Korean government (MSIT) RS-2025-00516815. J.Y. acknowledge the support from South China University of Technology the Fundamental Research Funds ofState Key Laboratory of Luminescent Materials and Devices (Skllmd-2025-14). J. Y. and R. L. Z. H. acknowledge funding from UK Research and Innovation for a Frontier Grant (no. EP/X029900/1), awarded via the 2021 European Research Council Starting Grant scheme. They also thank St. John's College, Oxford, for financial support through a Welcome Grant and Large Grant, as well as support from the John Fell/Oxford University Press Research Fund. R. L. Z. H. thanks the Royal Academy of Engineering and Science & Technology Facilities Council through the Senior Research Fellowship scheme (no. RCSRF/2324-18-68). Y.W. Zhang acknowledges funding from the National Key R&D Program of China No. 2023YFA1610000, National Natural Science Foundation of China under

Grant Number.12304036, and the Guangdong Basic and Applied Basic Research Foundation (2026A1515012397). R. X. acknowledges funding from Fundamental Research Funds for the Central Universities, Sun Yat-sen University Grant Code 74130–31610059. Funding for open access by the Universidade de Vigo/CISUG.

Conflicts of Interest

The authors declare no conflicts of interest.

Data Availability Statement

The data that support the findings of this study are available from the corresponding author upon reasonable request.

References

1. A. Dey, J. Ye, A. De, et al., "State of the Art and Prospects for Halide Perovskite Nanocrystals," *ACS nano* 15 (2021): 10775–10981, https://doi.org/10.1021/acsnano.0c08903.

2. Z. Chen, R. L. Z. Hoye, H.-L. Yip, et al., "Roadmap on Perovskite Light-emitting Diodes," *Journal of Physics: Photonics* 6 (2024): 032501, https://doi.org/10.1088/2515-7647/ad46a6.

3. J. S. Manser, J. A. Christians, and P. V. Kamat, "Intriguing Optoelectronic Properties of Metal Halide Perovskites," *Chemical Reviews* 116 (2016): 12956–13008, https://doi.org/10.1021/acs.chemrev.6b00136.

4. M. V. Kovalenko, L. Protesescu, and M. I. Bodnarchuk, "Properties and Potential Optoelectronic Applications of Lead Halide Perovskite Nanocrystals," *Science* 358 (2017): 745–750, https://doi.org/10.1126/science.aam7093.

5. C. Zou, Z. Ren, K. Hui, et al., "Electrically Driven Lasing From a Dual-cavity Perovskite Device," *Nature* 645 (2025): 369–374, https://doi.org/10.1038/s41586-025-09457-2.

6. J. Ye, N. Mondal, B. P. Carwithen, et al., "Extending the Defect Tolerance of Halide Perovskite Nanocrystals to Hot Carrier Cooling Dynamics," *Nature Communications* 15 (2024): 8120, https://doi.org/10.1038/s41467-024-52377-4.

7. J. Ye, M. M. Byranvand, C. O. Martínez, R. L. Z. Hoye, M. Saliba, and L. Polavarapu, "Defect Passivation in Lead-Halide Perovskite Nanocrystals and Thin Films: Toward Efficient LEDs and Solar Cells," *Angewandte Chemie* 60 (2021): 21636–21660, https://doi.org/10.1002/anie.202102360.

8. D. P. Nenon, K. Pressler, J. Kang, et al., "Design Principles for Trap-Free $CsPbX_3$ Nanocrystals: Enumerating and Eliminating Surface Halide Vacancies With Softer Lewis Bases," *Journal of the American Chemical Society* 140 (2018): 17760–17772, https://doi.org/10.1021/jacs.8b11035.

9. A. Buin, R. Comin, J. Xu, A. H. Ip, and E. H. Sargent, "Halide-Dependent Electronic Structure of Organolead Perovskite Materials," *Chemistry of Materials* 27 (2015): 4405–4412, https://doi.org/10.1021/acs.chemmater.5b01909.

10. Y. Li, C. Zhang, X. Zhang, et al., "Intrinsic Point Defects in Inorganic Perovskite $CsPbI_3$ From First-principles Prediction," *Applied Physics Letters* 111 (2017): 162106, https://doi.org/10.1063/1.5001535.

11. R. Grisorio, D. Conelli, R. Giannelli, et al., "A New Route for the Shape Differentiation of Cesium Lead Bromide Perovskite Nanocrystals With Near-unity Photoluminescence Quantum Yield," *Nanoscale* 12 (2020): 17053–17063, https://doi.org/10.1039/D0NR04246C.

12. Y. Feng, H. Li, M. Zhu, et al., "Nucleophilic Reaction-Enabled Chloride Modification on $CsPbI_3$ Quantum Dots for Pure Red Light-Emitting Diodes With Efficiency Exceeding 26%," *Angewandte Chemie International Edition* 63 (2024): e202318777, https://doi.org/10.1002/anie.202318777.

13. A. Ghorai, S. Mahato, S. Singh, et al., "Ligand-Mediated Revival of Degraded α-$CsPbI_3$ to Stable Highly Luminescent Perovskite," *Angewandte Chemie International Edition* 62 (2023): e202302852, https://doi.org/10.1002/anie.202302852.

14. J. Ye, C. Nicholls, W. H. Jeong et al., "Stronger Lewis Base Antisolvents Improve Perovskite Nanocrystal Stability," *ACS Energy Letters* (2026), https://doi.org/10.1021/acsenergylett.6c00480.

15. B. J. Bohn, Y. Tong, M. Gramlich, et al., "Boosting Tunable Blue Luminescence of Halide Perovskite Nanoplatelets Through Postsynthetic Surface Trap Repair," *Nano Letters* 18 (2018): 5231–5238, https://doi.org/10.1021/acs.nanolett.8b02190.

16. H. Lin, J.-Y. Dong, Q. Wei, et al., "Chelating Ligand Surface Functionalization for Ultrastable Efficient Blue Emissive Nanoplatelets," *ACS Materials Letters* 7 (2024): 59–67, https://doi.org/10.1021/acsmaterialslett.4c02269.

17. S. Sun, M. Lu, Y. Zhong, et al., "Bifunctional Molecule Enables High-Quality $CsPb(Br/Cl)_3$ Nanocrystals for Efficient and Stable Pure-Blue Perovskite Light-Emitting Diodes," *ACS Energy Letters* 7 (2022): 3974–3981, https://doi.org/10.1021/acsenergylett.2c01783.

18. W. Zhang, X. Li, C. Peng, et al., "CsPb(Br/Cl)3 Perovskite Nanocrystals With Bright Blue Emission Synergistically Modified by Calcium Halide and Ammonium Ion," *Nanomaterials* 12 (2022): 2026, https://doi.org/10.3390/nano12122026.

19. C. Otero-Martínez, J. Ye, J. Sung, et al., "Colloidal Metal-Halide Perovskite Nanoplatelets: Thickness-Controlled Synthesis, Properties, and Application in Light-Emitting Diodes," *Advanced Materials* 34 (2022): 2107105, https://doi.org/10.1002/adma.202107105.

20. X. Yang, L. Ma, M. Yu, et al., "Focus on perovskite emitters in blue light-emitting diodes," *Light Science and Applications* 12, (2023): 177, https://doi.org/10.1038/s41377-023-01206-2.

21. L. Protesescu, S. Yakunin, M. I. Bodnarchuk, et al., "Nanocrystals of Cesium Lead Halide Perovskites ($CsPbX_3$, X = Cl, Br, and I): Novel Optoelectronic Materials Showing Bright Emission With Wide Color Gamut," *Nano Letters* 15 (2015): 3692–3696, https://doi.org/10.1021/nl5048779.

22. C. Otero-Martínez, N. Fiuza-Maneiro, and L. Polavarapu, "Enhancing the Intrinsic and Extrinsic Stability of Halide Perovskite Nanocrystals for Efficient and Durable Optoelectronics," *ACS Applied Materials and Interfaces* 14 (2022): 34291–34302, https://doi.org/10.1021/acsami.2c01822.

23. W. Yin, M. Li, W. Dong, X. Zhang, and W. Zheng, "Overcoming the Ambient Manufacturability-Performance Bottleneck in Perovskite Nanocrystal Emitters for Efficient Light-Emitting Diodes," *Angewandte Chemie International Edition* 62 (2023): e202303462, https://doi.org/10.1002/anie.202303462.

24. V. G. V. Dutt, S. Akhil, R. Singh, M. Palabathuni, and N. Mishra, "Year-Long Stability and Near-Unity Photoluminescence Quantum Yield of $CsPbBr_3$ Perovskite Nanocrystals by Benzoic Acid Post-treatment," *Journal of Physical Chemistry C* 126 (2022): 9502–9508, https://doi.org/10.1021/acs.jpcc.2c01467.

25. N. Fiuza-Maneiro, K. Sun, I. López-Fernández, S. Gómez-Graña, P. Müller-Buschbaum, and L. J. A. E. L. Polavarapu, "Ligand Chemistry of Inorganic Lead Halide Perovskite Nanocrystals," *ACS Energy Letters* 8 (2023): 1152–1191, https://doi.org/10.1021/acsenergylett.2c02363.

26. R. K. Behera, S. Das Adhikari, S. K. Dutta, A. Dutta, and N. Pradhan, "Blue-Emitting $CsPbCl_3$ Nanocrystals: Impact of Surface Passivation for Unprecedented Enhancement and Loss of Optical Emission," *Journal of Physical Chemistry Letters* 9 (2018): 6884–6891, https://doi.org/10.1021/acs.jpclett.8b03047.

27. X. Zheng, B. Chen, J. Dai, et al., "Defect Passivation in Hybrid Perovskite Solar Cells Using Quaternary Ammonium Halide Anions and Cations," *Nature Energy* 2 (2017): 17102.

28. D. Jia, J. Chen, M. Yu, et al., "Dual Passivation of $CsPbI_3$ Perovskite Nanocrystals With Amino Acid Ligands for Efficient Quantum Dot Solar Cells," *Small* 16 (2020): 2001772, https://doi.org/10.1002/smll.202001772.

29. V. G. V. Dutt, S. Akhil, and N. Mishra, "Enhancement of Photoluminescence and the Stability of $CsPbX_3$ (X = Cl, Br, and I) Perovskite Nanocrystals With Phthalimide Passivation," *Nanoscale* 13 (2021): 14442–14449, https://doi.org/10.1039/D1NR03916D.

30. H. Li, L. Tao, F. Huang, et al., "Enhancing Efficiency of Perovskite Solar Cells via Surface Passivation With Graphene Oxide Interlayer," *ACS Applied Materials and Interfaces* 9 (2017): 38967–38976, https://doi.org/10.1021/acsami.7b10773.

31. G. H. Ahmed, J. K. El-Demellawi, J. Yin, et al., "Giant Photoluminescence Enhancement in $CsPbCl_3$ Perovskite Nanocrystals by Simultaneous Dual-Surface Passivation," *ACS Energy Letters* 3 (2018): 2301–2307, https://doi.org/10.1021/acsenergylett.8b01441.

32. J. Zhang, C. Yin, F. Yang, et al., "Highly Luminescent and Stable $CsPbI_3$ Perovskite Nanocrystals With Sodium Dodecyl Sulfate Ligand Passivation for Red-Light-Emitting Diodes," *Journal of Physical Chemistry Letters* 12 (2021): 2437–2443, https://doi.org/10.1021/acs.jpclett.1c00008.

33. J. Y. Woo, Y. Kim, J. Bae, et al., "Highly Stable Cesium Lead Halide Perovskite Nanocrystals Through In Situ Lead Halide Inorganic Passivation," *Chemistry of Materials* 29 (2017): 7088–7092, https://doi.org/10.1021/acs.chemmater.7b02669.

34. Y. Wu, C. Wei, X. Li, et al., "In Situ Passivation of PbBr 64–Octahedra Toward Blue Luminescent $CsPbBr_3$ Nanoplatelets With Near 100% Absolute Quantum Yield," *ACS Energy Letters* 3 (2018): 2030–2037, https://doi.org/10.1021/acsenergylett.8b01025.

35. N. Fiuza-Maneiro, I. López-Fernández, J. Ye, et al., "Strategies to Maximize the Dopant-To-Exciton Emission Ratio in Mn-Doped $CsPbCl_3$ Nanocrystals," *Advanced Optical Materials* 13 (2025): e02815, https://doi.org/10.1002/adom.202502815.

36. S. Singh, A. Sen, S. L. Aneesha, et al., "Defect Passivation Strategies in Halide Perovskite Solar Cells and LEDs," *ACS Energy Letters* 11, no. 4 (2026): 3060–3120, https://doi.org/10.1021/acsenergylett.5c04238.

37. A. Dutta, R. K. Behera, P. Pal, S. Baitalik, and N. Pradhan, "Near-Unity Photoluminescence Quantum Efficiency for All $CsPbX_3$ (X=Cl, Br, and I) Perovskite Nanocrystals: A Generic Synthesis Approach," *Angewandte Chemie International Edition* 58 (2019): 5552–5556, https://doi.org/10.1002/anie.201900374.

38. Y. Zhang, X. Cheng, D. Tu, et al., "Engineering the Bandgap and Surface Structure of $CsPbCl_3$ Nanocrystals to Achieve Efficient Ultraviolet Luminescence," *Angewandte Chemie International Edition* 60 (2021): 9693–9698, https://doi.org/10.1002/anie.202017370.

39. N. Mondal, A. De, and A. Samanta, "Achieving Near-Unity Photoluminescence Efficiency for Blue-Violet-Emitting Perovskite Nanocrystals," *ACS Energy Letters* 4 (2019): 32–39, https://doi.org/10.1021/acsenergylett.8b01909.

40. N. Fiuza-Maneiro, J. Ye, S. K. Sharma, et al., "Unlocking Brightness in $CsPbCl_3$ Perovskite Nanocrystals: Screening Ligands and Metal Halides for Effective Deep Trap Passivation," *ACS Energy Letters* 10 (2025): 1623–1632, https://doi.org/10.1021/acsenergylett.5c00185.

41. T. B. Haward, V. J. Y. Lim, I. Cherniukh, M. I. Bodnarchuk, M. V. Kovalenko, and L. M. Herz, "Correlated Vibrational and Electronic Signatures of Surface Disorder in CsPbBr3 Nanocrystals," *ACS Nano* 19 (2025): 40159–40169.

42. J. Kline, S. Gallagher, B. F. Hammel, et al., "Emissive Traps Lead to Asymmetric Photoluminescence Line Shape in Spheroidal $CsPbBr_3$ Quantum Dots," *Nano Letters* 25 (2025): 5063–5070, https://doi.org/10.1021/acs.nanolett.4c04995.

43. N. Pradhan, "Tips and Twists in Making High Photoluminescence Quantum Yield Perovskite Nanocrystals," *ACS Energy Letters* 4 (2019): 1634–1638, https://doi.org/10.1021/acsenergylett.9b00946.

44. P. M. A. Sherwood, "Introduction to Studies of Phosphorus-Oxygen Compounds by XPS," *Surface Science Spectra* 9 (2003): 62–66, https://doi.org/10.1116/11.20030101.

45. D. Ma, P. Todorović, S. Meshkat, et al., "Chloride Insertion–Immobilization Enables Bright, Narrowband, and Stable Blue-Emitting Perovskite Diodes," *Journal of the American Chemical Society* 142 (2020): 5126–5134, https://doi.org/10.1021/jacs.9b12323.

46. X. Liu, J. Zhang, H. Wang, et al., "CsPbI3 Perovskite Solar Module With Certified Aperture Area Efficiency >18% Based on Ambient-moisture-assisted Surface Hydrolysis," *Joule* 8 (2024): 2851–2862, https://doi.org/10.1016/j.joule.2024.06.026.

47. M. M. Achmatowicz, O. R. Thiel, J. T. Colyer, et al., "Hydrolysis of Phosphoryl Trichloride ($POCl_3$): Characterization, In Situ Detection, and Safe Quenching of Energetic Metastable Intermediates," *Organic Process Research & Development* 14 (2010): 1490–1500, https://doi.org/10.1021/op1001484.

48. J. Ye, A. Ren, L. Dai, et al., "Direct Linearly Polarized Electroluminescence From Perovskite Nanoplatelet Superlattices," *Nature Photon* 18 (2024): 586–594, https://doi.org/10.1038/s41566-024-01398-y.

49. M. Kaiser, Y. Li, J. Schwenzer, et al., "How Free Exciton–exciton Annihilation Lets Bound Exciton Emission Dominate the Photoluminescence of 2D-perovskites Under High-fluence Pulsed Excitation at Cryogenic Temperatures," *Journal of Applied Physics* 129 (2021): 123101, https://doi.org/10.1063/5.0037800.

50. A. Soni, D. Kushavah, L.-S. Lu, W.-H. Chang, and S. K. Pal, "Ultrafast Exciton Trapping and Exciton–Exciton Annihilation in Large-Area CVD-Grown Monolayer WS_2," *Journal of Physical Chemistry C* 125 (2021): 23880–23888, https://doi.org/10.1021/acs.jpcc.1c06267.

51. W. Deng, X. Jin, Y. Lv, X. Zhang, X. Zhang, and J. Jie, "2D Ruddlesden–Popper Perovskite Nanoplate Based Deep-Blue Light-Emitting Diodes for Light Communication," *Advanced Functional Materials* 29 (2019): 1903861, https://doi.org/10.1002/adfm.201903861.

52. C. Zhang, Q. Wan, L. K. Ono, et al., "Narrow-Band Violet-Light-Emitting Diodes Based on Stable Cesium Lead Chloride Perovskite Nanocrystals," *ACS Energy Letters* 6 (2021): 3545–3554, https://doi.org/10.1021/acsenergylett.1c01380.

53. Q. Hu, J. Guo, M. Lu, et al., "Efficient and Stable Mg_{2+} -Doped $CsPbCl_3$ Nanocrystals for Violet LEDs," *Journal of Physical Chemistry Letters* 12 (2021): 8203–8211, https://doi.org/10.1021/acs.jpclett.1c02416.

54. N. Wang, R. Sun, W. Xu, et al., "Enhanced Energy Transfer by Sb Ion Doping for Efficient $CsPbCl_3$: Mn_{2+} Perovskite Nanocrystals and Light Emitting Diodes," *Journal of Materials Chemistry C* 11 (2023): 1409–1417, https://doi.org/10.1039/D2TC03538C.

55. M. Hu, S. Fernández, Q. Zhou, et al., "Water Additives Improve the Efficiency of Violet Perovskite Light-emitting Diodes," *Matter* 6 (2023): 2356–2367, https://doi.org/10.1016/j.matt.2023.05.018.

56. M. Hu, J. Lyu, N. Murrietta, et al., "2D Mixed Halide Perovskites for Ultraviolet Light-emitting Diodes," *Device* 2 (2024):100511, https://doi.org/10.1016/j.device.2024.100511.

Supporting Information

Additional supporting information can be found online in the Supporting Information section.

Supporting File 1: anie72227-sup-0001-SuppMat.docx.